Conformational Relaxation Paths in Tryptamine

Marcel Böhm, Robert Brause,† Christoph Jacoby,‡ and Michael Schmitt*

Heinrich-Heine-Universität, Institut für Physikalische Chemie I, D-40225 Düsseldorf, Germany

Received: October 5, 2008; Revised Manuscript Received: November 14, 2008

The relative fluorescence intensities of three conformers of tryptamine have been determined as a function of stagnation pressure and nozzle temperature in a supersonic expansion. The relative intensities of the conformers that are connected by different direct and indirect interconversion paths on the potential-energy hypersurface differ considerably depending on the experimental conditions. The energies of the local minima and some transition states interconnecting them are studied on the ab initio level of theory. From the energies of the barriers and vibrational frequencies at the stationary points, conformer interconversion rates $k(T)$ and $k(E)$ have been obtained using statistical theories. In the cases experimentally observed here, vibrational cooling rates and interconversion rates must be of the same order of magnitude, while RRKM theory considerably overestimates $k(E)$ values, most probably due to an insufficient consideration of anharmonic coupling of the vibrational modes in tryptamine.

1. Introduction

Conformational relaxation in molecular beams is an important process which shifts population from higher energy conformers to lower energy conformers if the barrier separating the conformers is surmountable in early stages of the expansion. Apart from entropic effects,[1] this population transfer makes it difficult or even impossible to compare relative intensities of electronic origin bands with calculated ground-state energies of these conformers. Felder and Günthard[2] studied the conformational interconversion of *gauche*- and *trans*-1,2-difluoroethane in a molecular beam. These conformers are separated by a barrier of approximately 700 cm^{-1} and show strong interconversion, while 1,2-dichloroethane with a barrier of 1200 cm^{-1} does not show any population transfer. Ruoff et al. found a strong dependence of the conformational relaxation of the seed gas in the supersonic expansion. The most efficient relaxation takes place with argon as the carrier gas, while expansion in helium did not relax the higher energy form for barriers above 400 cm^{-1}.[3] In many studies of conformers the number of calculated low-energy conformers and observed bands in a supersonic jet experiment disagree.[4−8] Baer and Potts[9] studied the competition between conformational and vibrational relaxation and could show that insufficient consideration of anharmonic coupling of the vibrational modes leads to interconversion rates that are orders of magnitude below the statistical rates. Sturdy and Clary investigated the influence of anharmonicity on the conformational population of tryptamine. They stated that it seems likely that conformer interconversion occurs during the cooling phase in a supersonic expansion.[10]

The conformational landscape of tryptamine has been investigated extensively in several electronic states using a variety of experimental and theoretical methods.[11−22] To date seven different conformers of tryptamine have been identified and characterized experimentally. For the nomenclature of the different tryptamine conformers we use the scheme proposed by Carney et al.[15] The conformers in which the amino function of the ethylamino group is in the gauche position to the phenyl (pyrrole) ring are called Gph (Gpy). Conformers in which the ethylamino group is pointing away from the indole chromophore are called Anti. The orientation of the amino lone pair is given by the descriptor "up", "ph", "py", "out", and "in" depending on whether the lone pair points upward, to the phenyl side, to the pyrrole side, away from the indole ring, or down to the indole ring. In a series of high-resolution electronic spectroscopy studies the group of Pratt succeeded in assigning all seven conformers to experimentally observed bands.[19,22] At the same time, our group investigated the tryptamine and tryptamine−water system, but under comparable experimental conditions only six different conformer bands for the monomer were present.[20] The "missing" band, which is spectrally close to the origin of the C band of tryptamine and will be called C(2) in the following, has been reported by the groups of Levy,[12,13] Zwier,[15] and Pratt.[19] There has been disagreement in the assignment of the D band whether it is due to the Anti(py)[20] or Anti(ph)[19] conformer. Recent experiments in helium droplets showed that the D band must be assigned to the Anti(ph) conformer.[23] Consequently, the *C*(2) conformer has to be attributed to the Anti(py) conformer. The C(1) band has been assigned to the Gph(out) conformer. From a tunneling splitting in the C(2) and the D band Nguyen et al. concluded that the Anti(py) and Anti(ph) conformers are interconverted by a large amplitude motion.[19] The saddle points connecting the nine most stable conformers on the tryptamine hypersurface have been characterized theoretically at the B3LYP/6-31+G(d) level and compared to barriers that have been measured using stimulated emission pumping hole-filling spectroscopy (SEP-HFS).[21]

In the following we will study (i) the reason for the strong variations of the intensity ratio of the C(1)/C(2) bands in our rotationally resolved electronic spectra of tryptamine, (ii) the interconversion paths for the Gph(out), Anti(py), and Anti(ph) conformers, and (iii) the relaxation between these conformations in the molecular beam.

* To whom correspondence should be addressed. E-mail: mschmitt@uni-duesseldorf.de.

† Current address: Siltronic AG, 84489 Burghausen, Germany.

‡ Current address: Institut für Herz- und Kreislaufphysiologie, 40225 Düsseldorf, Germany.

10.1021/jp8087989 CCC: $40.75
Published on Web 12/17/2008

TABLE 1: MP2/6-311G(d,p) Energies of Several Stationary Points on the Potential-Energy Surface of Tryptamine[a]

structure	exp.	MP2 energies, Hartree	ZPE, Hartree	total energy, kJ/mol	relative energy, cm^{-1}	
Gph(out)	C(1)	−496.430790	0.203794	−1302843.978	0	
Anti(py)	C(2)	−496.427789	0.203111	−1302837.894	509	
Anti(ph)	D	−496.427755	0.203125	−1302837.765	519	
Anti(up)	E	−496.428233	0.203258	−1302838.671	444	
IP		−496.425662	0.202556	−1302833.765	854	
TS(I)	C(2)D	−496.425169	0.202694	−1302832.109	992	484
TS(II)	DE	−496.423357	0.202666	−1302827.424	1384	940
TS(III)	EC(2)	−496.423559	0.202717	−1302827.821	1351	907
TS(IV)	C(1)C(2)	−496.422206	0.202601	−1302824.573	1622	1622
TS(V)	C(2)D	−496.418250	0.201214	−1302817.829	2186	1677

[a] For the structures of TS(I)−TS(IV) refer to Figures 1, 2, and 3. Relative energies in wavenumbers are given with respect to the lowest energy structure and additionally in the last column for the transition states relative to the conformer with the lower energy along a reaction path connecting two different minima via this TS.

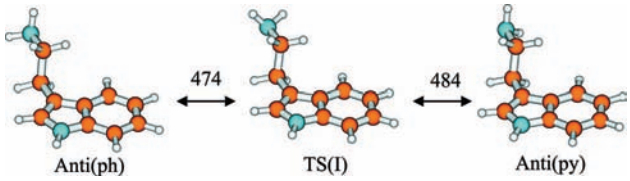

Figure 1. Direct interconversion paths between Anti(py) and Anti(ph).

2. Techniques

2.1. Experimental Methods. The experimental setup for the rotationally resolved laser-induced fluorescence is described in detail elsewhere.[24] In short, the vacuum system consists of three differentially pumped vacuum chambers that are linearly connected by two skimmers with orifice diameters of 1 and 2 mm in order to collimate the molecular beam and hence reduce the Doppler contribution to the measured line width to 25 MHz of full width at half-maximum (fwhm). The nozzle consists of a laser-drilled steel plug with a cylindrical orifice of 160 μm in the experiments described here. The laser system consists of a single-mode ring dye laser (Coherent 899-21) pumped with 7 W of the 514 nm line of an argon-ion laser (Coherent Innova 100). The fundamental of the dye laser is coupled into an external delta cavity (Spectra Physics) for second-harmonic generation (SHG) using an angle-tuned Brewster cut BBO crystal. The cavity length is locked to the dye laser frequency by a frequency modulation technique.[25,26] Typically, ∼40 mW of UV radiation is available for the experiment. The UV laser crosses the molecular beam 360 mm downstream from the nozzle under right angles. The molecular fluorescence is collected perpendicular to the plane defined by the laser and molecular beam by an imaging optics. The total fluorescence is detected by a photomultiplier tube whose output is digitized by a photon counter and passed to a PC for data acquisition and processing. The relative frequency is determined with a quasi-confocal Fabry−Perot interferometer. For the absolute frequency calibration an iodine spectrum is recorded and compared with the tabulated data.[27]

Because the C and the D bands are separated by 5 cm^{-1} they cannot be recorded in a single scan of the Coherent 899-21 ring laser, which is typically around 60 GHz (∼2 cm^{-1}) in the UV. Therefore, we had to paste together five subsequent scans, which had to provide sufficient overlap for a reliable intensity normalization of the single scans.

2.2. Theoretical Methods. ***2.2.1. Ab Initio Calculations.*** The stationary points on the tryptamine potential-energy surface (PES) have been optimized at the Møller−Plesset second-order perturbation theory (MP2/6-311G(d,p)) level with the Gaussian 03 program package.[28] The SCF convergence criterion used throughout the calculations is an energy change below 10^{-8} Hartree, while the convergence criterion for the gradient optimization of the molecular geometry was $\delta E/\delta r < 1.5 \times 10^{-5}$ Hartree/Bohr and $\delta E/\delta\phi < 1.5 \times 10^{-5}$ Hartree/deg, respectively. The vibrational frequencies were calculated using the analytical gradients. The transition states (TS) connecting the minima were optimized by the synchronous transit-guided quasi-Newton method (STQN),[29,30] implemented in the Gaussian03 program package.

2.2.2. Genetic Algorithms. We used an automated fitting procedure for determination of the molecular parameters best reproducing the rovibronic spectra based on a genetic algorithm fit, which is described in detail in refs 31–33.The GA library PGAPack version 1.0 was used, which can run on parallel processors.[34] For simulation of the rovibronic spectra a rigid asymmetric rotor Hamiltonian was employed.[35] The temperature dependence of the intensity is described by a two-temperature model

$$n(E, T_1, T_2, w) = e^{-E/kT_1} + we^{-E/kT_2} \quad (1)$$

where E is the energy of the lower state, k is the Boltzmann constant, w is a weighting factor, and T_1 and T_2 are the two temperatures.[36] The calculations were performed on 64 processors of an SGI Altix 3700 system. A typical fit with 64 processors takes less than 10 min. The genetic algorithm copies concepts from evolutionary processes like sexual reproduction, selection, and mutation. For a detailed description of the GA as fitting algorithms the reader is referred to the original literature on evolutionary or genetic algorithms.[37−39]

3. Results and Discussion

3.1. Theory. The most stable of the three Anti conformers at the MP2/6-311G(d,p) level of theory (including zero-point enery correction at the same level of theory) is the Anti(up) conformer. The energies of Anti(py) and Anti(ph) are slightly higher (+65 and + 76 cm^{-1}, respectively). Of the experimentally investigated conformers (C(1) ≡ Gph(out), C(2) ≡ Anti(py), and D ≡ Anti(ph)) in this study the Gph(out) conformer is the most stable one.

The calculated MP2/6-311G(d,p) barriers of several interconversion paths connecting the Gph(out) and the Anti(ph) and Anti(py) conformers of tryptamine are collected in Table 1. All stationary points contain zero-point vibrational energy corrections. Direct and indirect interconversion paths between the Anti(py) and Anti(ph) conformers were identified: The direct path represents the torsional motion about the C−N bond with an "Anti(down)" conformer representing the transition state (TS(I)) for this path, cf. Figure 1. If viewing from the side of

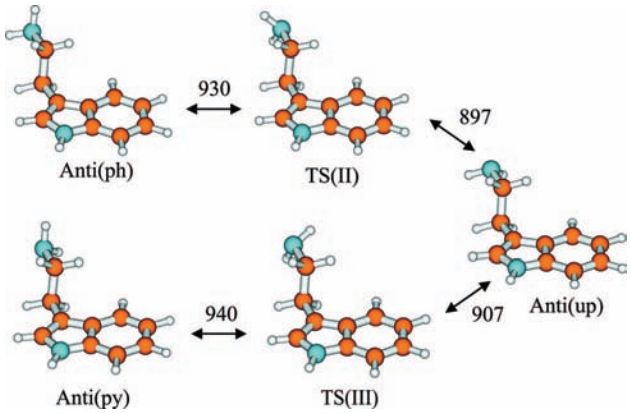

Figure 2. Indirect interconversion paths between Anti(py) and Anti(ph).

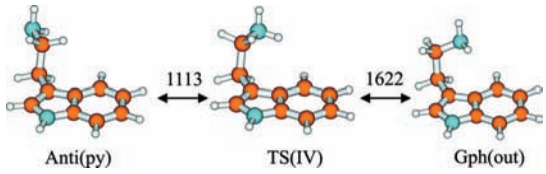

Figure 3. Interconversion path between Gph(out) and Anti(py).

the indole ring toward the C−N bond as in Figure 1, a clockwise rotation, starting from the Anti(ph) conformer (experimentally observed as the D conformer) by 60° leads to TS(I) and a further 60° rotation in the same direction to the Anti(py) conformer (experimentally observed as C(2) conformer).

Another direct path connecting the Anti(ph) and Anti(py) conformers was identified that consists of a simultaneous torsional and inversion motion of the amino group. This TS is situated nearly 1700 cm^{-1} above the minimum of the Anti(py) conformer and will not be considered here. Its energy is given in Table 1 as TS(V). It can be obtained together with all other stationary-point structures from the author's homepage at http://www-public.rz.uni-duesseldorf.de/~mschmitt/.

In the indirect path, shown in Figure 2, an anticlockwise rotation (same line of view as in the first case) by 60° starting from Anti(ph) leads to another eclipsed transition state (TS(II)). Further −60° rotation leads to the Anti(up) conformer, which represents again a stable minimum at the potential-energy surface (eperimentally determined as the E conformer). Two further successive 60° rotations are necessary to interconvert Anti(up) to Anti(py) over transition state TS(III).

The direct interconversion path between the Anti conformers (via TS(I)) has a considerably lower barrier (483.6 cm^{-1}) compared to the two barriers of the indirect interconversion paths (via TS(II) and TS(III)).

The Gph(out) conformer is connected via a clockwise rotation about the $C_\alpha-C_\beta$ bond of the ethylamino group with the Anti(py) conformer. TS(IV) is located at a 60° rotation relative to Gph(out); further 60° rotation leads to the stable Anti(py) minimum, cf. Figure 3.

The barrier for this direct path amounts to 1622 cm^{-1}, which is higher than both the direct and the indirect paths for the Anti(py) ↔ Anti(ph) interconversion.

3.2. Experiment. Figure 4 shows the complete scan from the beginning of the P branch of the C(1) conformer with its origin at 34879.22 cm^{-1} to the end of the R branch of the D conformer (origin at 34884.26 cm^{-1}) taken at a stagnation pressure of 250 mbar argon and a nozzle temperature of 217 °C. The lower traces show the simulated components of which

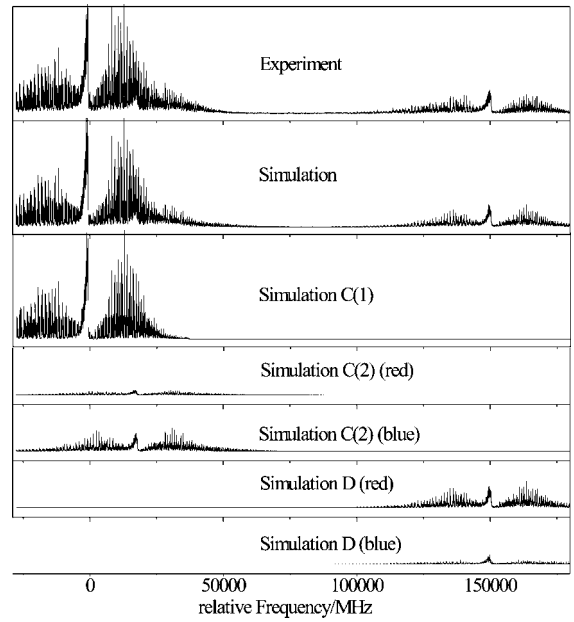

Figure 4. Rotationally resolved spectrum of the electronic origins of the *C* and *D* bands of tryptamine along with the simulations showing the constituent bands of the observed spectrum. The frequencies at the axis of abscissa are given relative to the origin of the strongest band, which is the Gph(out) conformer origin.

the spectrum is composed using the best molecular parameters from a GA fit. The molecular parameters obtained from the GA fit are given in Table 2. Along with the internal molecular parameters (rotational constants of the ground and excited electronic states, electronic origin, and orientation of the transition dipole moment) we also fit the rotational temperature and relative intensities of all bands in the observed spectral range. According to Nguyen and Pratt,[19] both the C(2) and the D band consist of two subbands split by 95 MHz. Thus, in the range of interest five vibronic bands have to be considered in the fit. The first band is the electronic origin of the C(1) conformer, the second is the red component of the C(2) band, the third the blue component of the same, the fourth is the red component of the D conformer, and the fifth is its blue component. Between the red and the blue components an intensity ratio of 1:3 for C(1) and 3:1 for the D conformer was determined by the GA fit, which is in accordance with ref 19.

3.3. Interconversion of C(2) and D. According to Nguyen and Pratt[19] there are two facts that are believed to strongly support the assumption that the C(2) and D conformers are directly interconverted. First, the intensity ratio of the red and blue subbands is 1:3 for the C(2) band and 3:1 for the D band, which they claimed to be the signature of the permutation of the two amino hydrogen atoms. Second, the splitting of both the C(2) and the D bands amounts to exactly 95 MHz. Since this experimentally observed splitting is caused by the difference of the ground-state and excited-state splitting an incidental equality would be rather improbable.

The conformational interconversion alone cannot cause the observed splittings and spin statistics because the two conformers which are connected via the torsional barrier described in section 3.1 have different energies. Therefore, Nguyen and Pratt[19] made a coupled two-dimensional motion along torsion and inversion coordinates responsible for the observed spectral features.

A different explanation for the observed splittings might be found in the interconversion between the two enatiomers, which

TABLE 2: Parameters from the Best GA Fit Used for Simulation of the Tryptamine Spectrum, Shown in Figure 4[a]

	Gph(out), C(1)	Anti(py)(I), C(2)(red)	Anti(py)(II), C(2)(blue)	Anti(ph)(I), D(red)	Anti(ph)(II), D(blue)
A/MHz	1590.07	1776.28	1779.65	1767.97	1768.65
B/MHz	754.94	616.01	615.15	618.39	617.74
C/MHz	561.18	478.21	476.18	478.27	476.72
Δ*A*/MHz	−6.75	−16.03	−14.32	−14.85	−13.77
Δ*B*/MHz	−12.71	−5.86	−5.20	−6.15	−5.42
Δ*C*/MHz	−7.20	−5.34	−3.50	−4.93	−3.54
ϕ/deg	88.20	59.88	74.08	44.84	72.75
θ/deg	0.44	46.14	43.01	39.49	38.48
ν_0/cm^{-1}	34879.22	34879.83	34879.84	34884.26	34884.26
$\Delta\nu_0$/MHz	0.00	18410.4	18505.4	151112.0	151207.0
T_1/K	4.36	4.36	4.36	4.36	4.36
T_2/K	5.05	5.05	5.05	5.05	5.05
weight	0.04	0.04	0.04	0.04	0.04
rel. int.	1.00	0.08	0.25	0.27	0.09

[a] ν_0 gives the absolute electronic origin from comparison to the tabulated lines of the iodine spectrum, while $\Delta\nu_0$ gives the much more accurate frequency differences of the electronic origins, which are obtained directly from the GA fit.

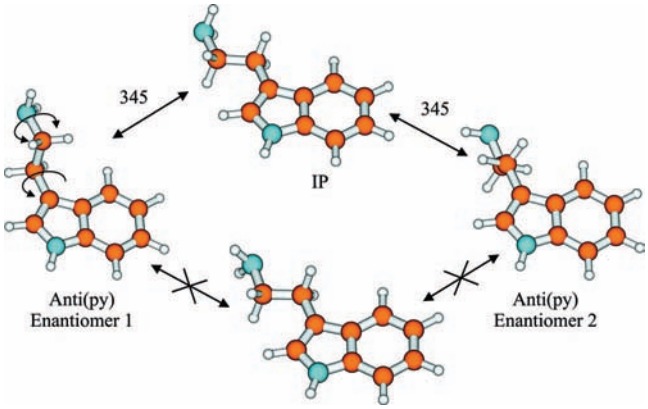

Figure 5. Two different interconversion paths, which interconvert the two Anti(py) enantiomers differing in the orientation (above or below) of the ethyl amino side chain with respect to the aromatic plane.

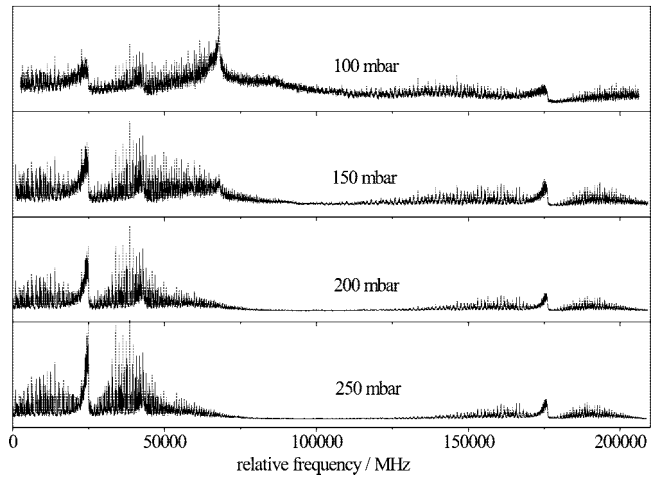

Figure 6. Rotationally resolved spectra of the *C* and the *D* bands of tryptamine at four different stagnation pressures.

differ in the ethylamino side chain orientation with respect to the indole plane ("above" and "below"). In addition to the transition states that connect different conformers we also calculated the structure which results when the ethylamino side chain of the D conformer is rotated into the indole plane (cf. Figure 5). This in-plane (IP) structure is again a local minimum at the PES of tryptamine with an energy of 854 cm^{-1} above the Gph(out) energy and 345 cm^{-1} above the Anti(py) minimum (IP in Table 1). Thus, the interconversion of the enantiomers would be indirect via an intermediate stable species. The motion, which interconnects the two Anti(py) enantiomers (and of course equally the two Anti(ph) enantiomers), is a coupled rotation of the ethylamino side chain about the $C_\alpha C_\beta$ and $C_\gamma N$ bonds. Two different relative senses of rotations are possible: both rotate in the opposite direction (upper path in Figure 5) or rotate in the same direction (lower path in Figure 5). For the $C_\alpha C_\beta$ bond only counterclockwise rotation is possible due to steric hindrance. Rotation in the same direction does not lead to a converged structure most likely due to steric hindrance between the C_γ hydrogen atoms and the amino hydrogens. The energy of the in-plane conformer IP is only 345 cm^{-1} above the Anti(py) minimum. If the barriers in the excited states are sufficiently small the observed splitting of 95 MHz might also be explained by this motion despite the very small torsional constant *F* for this motion.

As for the different spin statistics in both bands, no definite statement can be made. The interchange of the 1:3 spin statistical weights for the red and blue components might be due to the interchange of the tunneling components.

3.4. Pressure Dependence of the Relative Intensities. We recorded the spectrum in the same range at different stagnation pressures and nozzle temperatures. At a stagnation pressure of 400 mbar both Anti spectra (C(2) and D) nearly vanish. Figure 6 shows the spectrum as a function of the argon stagnation pressure in the range between 100 and 250 mbar. The most striking differences in the appearance of the spectra at different

TABLE 3: Dependence of the Relative Intensities of the Various Conformers of Tryptamine Shown in Figure 6 on the Stagnation Pressure

	Gph(out), C(1)	Anti(py)(I), C(2)(red)	Anti(py)(II), C(2)(blue)	Anti(ph)(I), D(red)	Anti(ph)(II), D(blue)
100 mbar	1.00	0.12	0.35	0.13	0.40
150 mbar	1.00	0.11	0.33	0.11	0.34
200 mbar	1.00	0.08	0.23	0.08	0.23
250 mbar	1.00	0.06	0.18	0.07	0.21

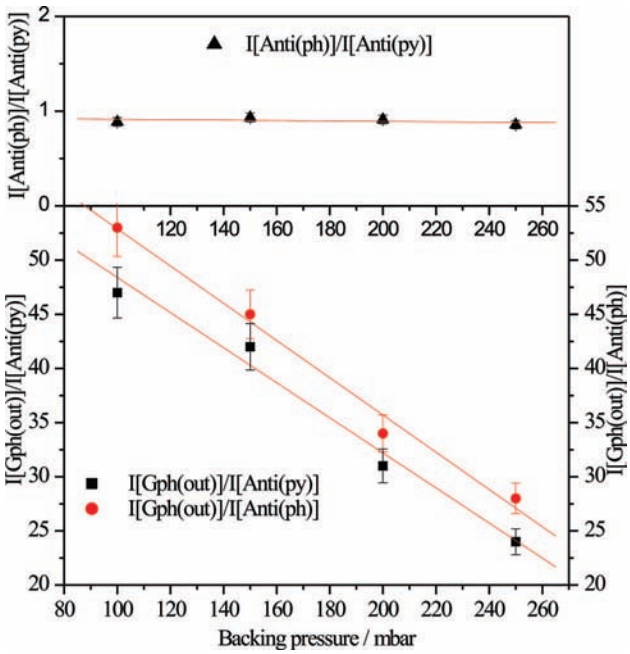

Figure 7. Variation of the intensity ratios of the Gph(out), Anti(py) and Anti(ph) conformers of tryptamine with the stagnation pressure.

pressures are due to the (rotational) temperature differences in the molecular beam. At 250 mbar a rotational temperature of about 4 K is obtained from the fit, while at 100 mbar the temperature raises to 17 K. The fit of the 250 mbar spectrum requires a maximum of rotational quanta J_{max} in the calculations of 60 to be taken into account, while at 100 mbar the maximum of J raises to 140. Since the computation time for the simulation of a single spectrum goes with J^2, the fit of the spectrum at 100 mbar takes more than five times longer than at 250 mbar.

The ratio of the intensities of the Gph(out) (C(1)) band and the Anti conformers (C(2) and D) gradually shifts toward smaller values with decreasing pressure. Table 3 gives the relative intensities of the observed bands from the results of the GA fit. Since no absolute intensities can be fit the intensity of the first band (C1) in the calculated range is set to 1, and the intensities of the stronger components of C(2) and D are calculated relative to this band. The intensities of the weaker components are calculated relative to those of the stronger component. In both cases, an exact ratio of 0.33 is found at all pressures for C(2)(red)/C(2)(blue) and D(blue)/D(red), respectively, supporting the original assumption of Nguyen et al. that the appearance of two components in the spectrum of the Anti conformers is caused by a splitting due to a large amplitude motion.[19]

The intensity ratios of Anti(ph)/Anti(py), Gph(out)/Anti(py), and Gph(out)/Anti(ph) are calculated taking the sum of the intensities of both tunneling components of the Anti conformers into account and are plotted versus the backing pressure in Figure 7. Obviously, the ratio of the two Anti conformers only changes slightly upon variation of the expansion conditions. On the other hand, a large change occurs regarding the ratios of the Gph(out) intensity and the two Anti conformers. At 250 mbar backing pressure the fraction of the Anti(py) (C(2)) conformer to the total signal in the region of the strong Gph(out) (C(1)) band amounts to less than 20%. At a backing pressure of 600 mbar (corresponding to a rotational temperature of 2.5 K), at which these kinds of spectra are normally taken in our machine, there are no Anti(py) bands within a signal-to-noise ratio of 1000 detectable. Such a strong dependence of the conformational composition in the molecular beam from the

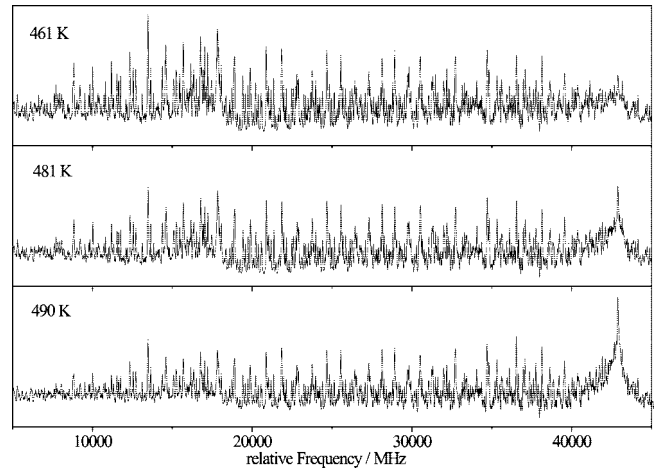

Figure 8. Rotationally resolved electronic spectra of the Gph(out) and Anti(py) conformers of tryptamine at different nozzle temperatures.

TABLE 4: Dependence of the Relative Intensities of the Gph(out) and Anti(py) Conformers of Tryptamine on the Nozzle Temperature

	Gph(out), C(1)	Anti(py)(I), C(2)(red)	Anti(py)(II), C(2)(blue)
461 K	1.00	0.12	0.37
481 K	1.00	0.13	0.39
490 K	1.00	0.12	0.38

stagnation pressure is very unusual and clearly puts strong limits to attempts of deriving stability information of various conformers in a molecular beam from their relative intensities as frequently found in the literature. Attempts to change the buffer gas to He or Ne in order to determine the degree of relaxation with these lighter noble gases failed due to the increased Doppler width in our beam machine when expanding with these buffer gases.

3.5. Temperature Dependence of the Relative Intensities. Depending on the energy difference of the Anti(ph) and Anti(py) conformer their intensities should vary with different nozzle temperatures. The fraction of the more stable conformer will decrease upon increasing temperature by the same amount as the less stable one increases. A plot of the logarithm of the intensity ratio of both bands versus the inverse absolute temperature yields the standard reaction enthalpy $\Delta H^{\ominus}$ for interconversion of the two tautomers from the slope, which equals $\Delta H^{\ominus}/R$. Application of this relation to conformer equilibria in molecular beams suffers from the problem that the temperature is not known. An instantaneous freezing of the conformer composition directly after expansion would imply a temperature equal to the nozzle temperature. Freezing, in this context, means that no passage over the barrier at the temperature under consideration occurs. For very high barriers this behavior can indeed be found, but even for medium size barriers conformer interconversion occurs in the course of expansion, leading to a lower temperature than that of the nozzle.

The change of the intensity ratio of Gph(out)/Anti(py) was recorded as a function of the nozzle temperature. The spectra taken at nozzle temperatures of 461, 481, and 490 K are shown in Figure 8. The relative intensities of the bands were determined from the GA fit as described in section 3.4 and given in Table 4.

The ratio of the sum of intensities of both Anti(py) components and the Gph(out) intensity is plotted as function of the inverse nozzle temperature in Figure 9. The sign of the gradient

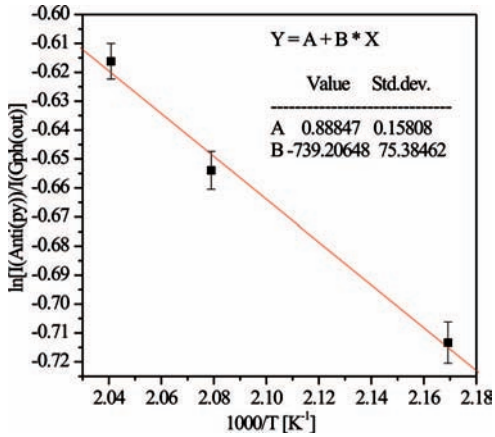

Figure 9. Plot of the logarithm of the intensity ratio of the Anti(py) and Gph(out) conformers of tryptamine vs the inverse absolute nozzle temperature.

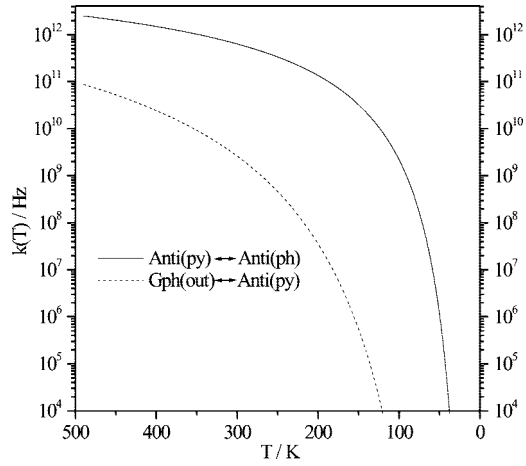

Figure 10. Logarithmic plot of $k(T)$ versus T for the interconversion of Anti(py) ↔ Anti(ph) and of Gph(out) ↔ Anti(py) calculated from eq 2.

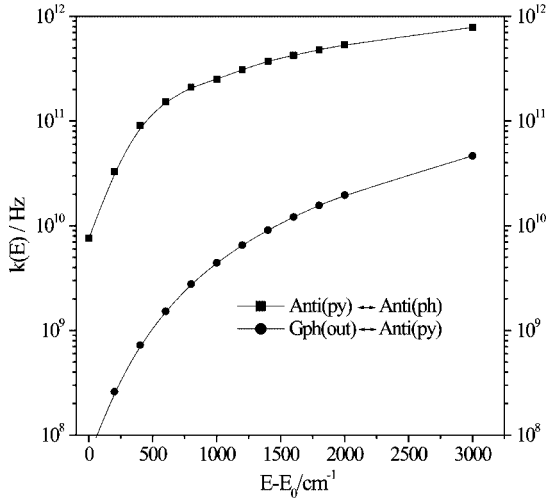

Figure 11. Logarithmic plot of $k(E)$ for the Anti(py) ↔ Anti(ph) and Gph(out) ↔ Anti(py) interconversions calculated from eq 3 vs the excess energy $E - E_0$ above the ZPE of the respective barrier.

in this van't Hoff plot immediately shows that the Gph(out) is the more stable conformer. From the slope the standard reaction enthalpy ΔH^{Θ} can be computed to be 6.14 kJ/mol (513 cm^{-1}), in good agreement with the results of the ab initio calculations shown in Table 1. This agreement indicates fast conformational

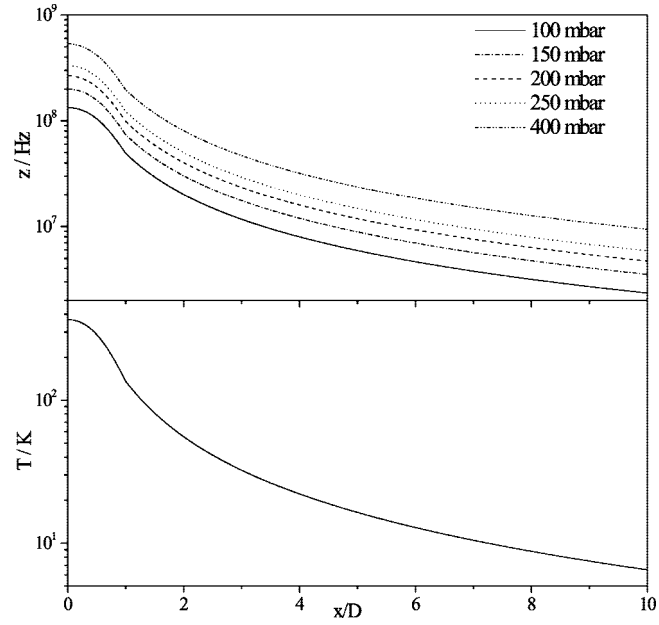

Figure 12. Logarithmic plot of the hard-sphere collision rate $z((x)/(D))$ and temperature in the molecular beam versus the reduced distance from the nozzle orifice.

freezing and therefore shows that vibrational relaxation rate in the expansion is larger than the interconversion rate.

3.6. Calculation of Statistical and RRKM Interconversion Rates. In the following a rough estimate of the statistical conformer interconverion rates and vibrational relaxation rates will be given. The conversion rates for the Anti(py) ↔ Anti(ph) and Gph(out) ↔ Anti(py) conformer interconversion have been calculated according to transition-state theory (TST)

$$k(T) = \frac{k_B T}{h} e^{-\Delta G^{\ddagger}/RT} \tag{2}$$

with the free energy of activation $\Delta G^{\ddagger}$, the Boltzman constant k_B, the Planck constant h, the molar gas constant R, and the absolute temperature T. At a temperature of 490 K (the upper limit in our investigations) an interconversion rate for Anti(py) ↔ Anti(ph) is calculated to be 2.5×10^{12} Hz using a $\Delta G^{\ddagger}$ of 484 cm^{-1} from the ab initio calculations. For the Gph(out) ↔ Anti(py) equilibrium $k(T)$ is found to be 8.7×10^{10} Hz ($\Delta G^{\ddagger}$ =1622 cm^{-1}). Both rates quickly drop with decreasing nozzle temperature as shown in Figure 10.

The microcanonical rates of interconversion were also calculated using the RRKM equation

$$k(E) = \frac{N^{\ddagger}(E - E_0)}{h\rho(E)} \tag{3}$$

where $N^{\ddagger}(E - E_0)$ is the sum of all states of the transition state in the energy range between its zero-point vibrational energy (ZPE) level and $E - E_0$. This sum is readily calculated from the relation

$$N^{\ddagger}(E - E_0) = \int_0^{E-E_0} \rho^{\ddagger}(E)\, dE \tag{4}$$

where $\rho(E)$ and $\rho^{\ddagger}(E)$ are the densities of states of the reactants and transition state at the energy E, respectively. Calculation of the sum of states $N^{\ddagger}(E - E_0)$ and density of states $\rho(E)$ was done by exact count of the number of states and alternatively using the quasi-exact Beyer−Swinehart−Stein−Rabinovitch algorithm from ref 40 with an energy resolution of 0.5 cm^{-1} using a computer program written by Daniel Spangenberg.[41]

The vibrational frequencies calculated at the MP2/6-311G(d,p)-optimized stationary points (minima and transition states) were used for the state count. Figure 11 shows the results for $k(E)$ at different energies $E - E_0$ for the Anti(py) ↔ Anti(ph) and Gph(out) ↔ Anti(py) interconversions.

These interconversion rates obtained from TST and RRKM theory have to be compared to the vibrational relaxation rates in the molecular beam.

Figure 12 shows how the hard-sphere collision rate of argon decreases with increasing distance from the nozzle orifice.[42] In the case where all collisional energy is converted into vibrational energy, the collision rate equals the cooling rate. Thus, the collision rate is the upper limit to the vibrational cooling rate. In general, the cooling rate will be much lower due to imperfect energy transfer. Since the conformer interconversion rates from statistical theory are more than 3 orders of magnitude larger than the collision rates, we conclude that conformational freezing takes place on a faster time scale than vibrational cooling. An overestimation of statistical reaction rates of 3 orders of magnitudes is known from other isomerization processes like in 2-fluoroethanol[43] or methyl and ethyl cyclohexanones.[10] In these cases a slow IVR has been made responsible for overestimation of rates by RRKM theory. Even when taking into account this overestimation of statistical reaction rates, cooling is slow in the examples studied here compared to conformational relaxation.

4. Conclusions

We performed experiments concerning the interconversion of various tryptamine conformers in a molecular beam. Strong dependence of the conformerical composition of the beam on the expansion conditions like stagnation pressure and nozzle temperature and also on the nozzle dimensions were found. If vibrational cooling was fast with respect to conformational relaxation, the ratio of the conformer concentrations as present at the nozzle temperature would be frozen out. If, on the other hand, the conformational relaxation is faster, the cooling leads to relaxation into only the most stable conformer(s). We have shown that interconversion of the Gph(out) conformer of tryptamine into the Anti(py) conformer in a molecular beam experiment closely follows a van't Hoff behavior at nozzle temperature. Therefore, we conclude that little vibrational cooling takes place at the time scale of the conformational interconversion. This behavior is confirmed by an estimation of the statistical interconversion and vibrational cooling rates.

Acknowledgment. This work was performed in the SFB 663 TP A2, Universität Düsseldorf, and printed upon its demand with financial support from the Deutsche Forschungsgemeinschaft. This work is part of the Ph.D. Thesis of Marcel Böhm.

References and Notes

(1) Kaczor, A.; Reva, I. D.; Proniewicz, L. M.; Fausto, R. Importance of Entropy in the Conformational Equilibrium of Phenylalanine: A Matrix-Isolation Infrared Spectroscopy and Density Functional Theory Study. *J. Phys. Chem. A* **2006**, *110*, 2360.

(2) Felder, P.; Günthard, H. H. Conformational interconversions in supersonic jets: matrix IR spectroscopy and model calculations. *Chem. Phys.* **1982**, *71*, 9.

(3) Ruoff, R. S.; Klots, T. D.; Emilsson, T.; Gutowski, H. S. Relaxation of conformers and isomers in seeded supersonic jets of inert gases. *J. Chem. Phys.* **1990**, *93*, 3142.

(4) Godfrey, P. D.; Brown, R. D.; Rogers, F. M. The missing conformers of glycine and alanine: relaxation in seeded supersonic jets. *J. Mol. Struct.* **1996**, *376*, 65.

(5) Godfrey, P. D.; Brown, R. D. Proportions of Species Observed in Jet Spectroscopy-Vibrational Energy Effects: Histamine Tautomers and Conformers. *J. Am. Chem. Soc.* **1998**, *120*, 10724.

(6) Nir, E.; Janzen, C.; Imhof, P.; Kleinermanns, K.; de Vries, M. S. Guanine tautomerism revealed by UV-UV and IR-UV hole burning spectroscopy. *J. Chem. Phys.* **2001**, *115*, 4604.

(7) Piuzzi, F.; Mons, M.; Dimicoli, I.; Tardivel, B.; Zhao, Q. Ultraviolet spectroscopy and tautomerism of the DNA base guanine and its hydrate formed in a supersonic jet. *Chem. Phys.* **2001**, *270*, 205.

(8) Fraser, G. T.; Suenram, R. D.; Lugez, C. L. Investigation of conformationally rich molecules: Rotational spectra of fifteen conformational isomers of 1-octene. *J. Phys. Chem. A* **2001**, *105*, 9859.

(9) Baer, T.; Potts, A. R. Nonstatistical chemical reactions: The isomerization over low barriers in methyl and ethyl cyclohexane. *J. Phys. Chem. A* **2000**, *104*, 9397.

(10) Sturdy, Y. K.; Clary, D. C. Torsional anharmonicity in the conformational analysis of tryptamine. *J. Phys. Chem. A.* **2007**, *9*, 2065.

(11) Sipior, J.; Sulkes, M. Conformational analysis of jet cooled tryptophan analogs by molecular mechanics: Comparison with experiment. *J. Chem. Phys.* **1993**, *98*, 6146.

(12) Park, Y. D.; Rizzo, T. R.; Peteanu, L. A.; Levy, D. H. Electronic spectroscopy of tryptophan analogs in supersonic jets: 3-Indole acetic acid, 3-indole propionic acid, tryptamine, and N-acetyl tryptophan ethyl ester. *J. Chem. Phys.* **1986**, *84*, 6539.

(13) Philips, L. A.; Levy, D. H. Rotationally resolved electronic spectroscopy of tryptamine conformers in a supersonic jet. *J. Chem. Phys.* **1988**, *89*, 85.

(14) Connell, L. L.; Corcoran, T. C.; Joireman, P. W.; Felker, P. M. Conformational analysis of jet-cooled tryptophan analogs by rotational coherence spectroscopy. *Chem. Phys. Lett.* **1990**, *166*, 510.

(15) Carney, J. R.; Zwier, T. S. The Infrared and Ultraviolet Spectra of Individual Conformational Isomers of Biomolecules: Tryptamine. *J. Phys. Chem. A* **2000**, *104*, 8677.

(16) Dian, B. C.; Longarte, A.; Zwier, T. S. Hydride stretch infrared spectra in the excited electronic states of indole and its derivatives: Direct evidence for the 1 ps* state. *J. Chem. Phys.* **2003**, *118*, 2696.

(17) Caminati, W. The rotational spectra of conformers of biomolecules: tryptamine. *Phys. Chem. Chem. Phys.* **2004**, *6*, 2806.

(18) Dian, B. C.; Clarkson, J.; Zwier, T. S. Direct measurement of Energy Thresholds to Conformational Isomerization of Tryptamine. *Science* **2004**, *303*, 1169.

(19) Nguyen, T.; Korter, T.; Pratt, D. Tryptamine in the gas phase. A high resolution laser study of the structural and dynamic properties of its ground and electronically excited states. *Mol. Phys.* **2005**, *103*, 1603.

(20) Schmitt, M.; Böhm, M.; Ratzer, C.; Vu, C.; Kalkman, I.; Meerts, W. L. Structural selection by microsolvation: conformational locking of tryptamine. *J. Am. Chem. Soc.* **2005**, *127*, 10356.

(21) Clarkson, J. R.; Dian, B. C.; Moriggi, L.; DeFusco, A.; McCarthy, V.; Jordan, K. D.; Zwier, T. S. Direct measurement of the energy thresholds to conformational isomerization in Tryptamine: Experiment and theory. *J. Chem. Phys.* **2005**, *122*, 214211.

(22) Nguyen, T.; Pratt, D. Permanent electric dipole moments of four tryptamine conformers in the gas phase: A new diagnostic of structure and dynamics. *J. Chem. Phys.* **2006**, *124*, 054317.

(23) Pei, L.; Zhang, J.; Wu, C.; Kong, W. Conformational identification of tryptamine embedded in superfluid helium droplets using electronic polarization spectroscopy. *J. Chem. Phys.* **2006**, *125*, 024305.

(24) Schmitt, M.; Küpper, J.; Spangenberg, D.; Westphal, A. Determination of the structures and barriers to hindered internal rotation of the phenol-methanol cluster in the S_0 *and* S_1 state. *Chem. Phys.* **2000**, *254*, 349.

(25) Pound, R. Electronic stabilization of microwave ocillators. *Rev. Sci. Instrum.* **1946**, *17*, 490.

(26) Drewer, R.; Hall, J.; Kowalski, F.; Hough, J.; Ford, G.; Munley, A.; Ward, H. Laser phase and frequency stabilization using an optical resonator. *Appl. Phys. B: Laser Opt.* **1983**, *31*, 97.

(27) Gerstenkorn, S.; Luc, P. *Atlas du spectre d'absorption de la molécule d'iode 14800−20000 cm*$^{-1}$; CNRS: Paris, 1986.

(28) Frisch, M. J.; Trucks, G. W.; Schlegel, H. B.; Scuseria, G. E.; Robb, M. A.; Cheeseman, J. R.; Montgomery, J. A., Jr.; Vreven, T.; Kudin, K. N.; Burant, J. C.; Millam, J. M.; Iyengar, S. S.; Tomasi, J.; Barone, V.; Mennucci, B.; Cossi, M.; Scalmani, G.; Rega, N.; Petersson, G. A.; Nakatsuji, H.; Hada, M.; Ehara, M.; Toyota, K.; Fukuda, R.; Hasegawa, J.; Ishida, M.; Nakajima, T.; Honda, Y.; Kitao, O.; Nakai, H.; Klene, M.; Li, X.; Knox, J. E.; Hratchian, H. P.; Cross, J. B.; Adamo, C.; Jaramillo, J.; Gomperts, R.; Stratmann, R. E.; Yazyev, O.; Austin, A. J.; Cammi, R.; Pomelli, C.; Ochterski, J. W.; Ayala, P. Y.; Morokuma, K.; Voth, G. A.; Salvador, P.; Dannenberg, J. J.; Zakrzewski, V. G.; Dapprich, S.; Daniels, A. D.; Strain, M. C.; Farkas, O.; Malick, D. K.; Rabuck, A. D.; Raghavachari, K.; Foresman, J. B.; Ortiz, J. V.; Cui, Q.; Baboul, A. G.; Clifford, S.; Cioslowski, J.; Stefanov, B. B.; Liu, G.; Liashenko, A.; Piskorz, P.; Komaromi, I.; Martin, R. L.; Fox, D. J.; Keith, T.; Al-Laham, M. A.; Peng, C. Y.; Nanayakkara, A.; Challacombe, M.; Gill, P. M. W.; Johnson,

B.; Chen, W.; Wong, M. W.; Gonzalez, C.; Pople, J. A. *Gaussian 03*, Revision A.1; Gaussian, Inc.: Pittsburgh, PA, 2003.

(29) Peng, C.; Ayala, P. Y.; Schlegel, H. B.; Frisch, M. J. Using redundant internal coordinates to optimize geometries and transition states. *J. Comput. Chem.* **1996**, *17*, 49.

(30) Peng, C.; Schlegel, H. B. Combining Synchronous Transit and Quasi-Newton Methods for Finding Transition States. *Isr. J. Chem.* **1994**, *33*, 449.

(31) Hageman, J. A.; Wehrens, R.; de Gelder, R.; Meerts, W. L.; Buydens, L. M. C. Direct determination of molecular constants from rovibronic spectra with genetic algorithms. *J. Chem. Phys.* **2000**, *113*, 7955.

(32) Meerts, W. L.; Schmitt, M.; Groenenboom, G. New applications of the Genetic Algorithm for the interpretation of High Resolution Spectra. *Can. J. Chem.* **2004**, *82*, 804.

(33) Meerts, W. L.; Schmitt, M. Application of genetic algorithms in automated assignments of high-resolution spectra. *Int. Rev. Phys. Chem.* **2006**, *25*, 353.

(34) Levine, D. PGAPack V1.0, PGAPack can be obtained via anonymous ftp from: ftp://ftp.mcs.anl.gov/pub/pgapack/pgapack.tar.Z, 1996.

(35) Allen, H. C.; Cross, P. C. *Molecular Vib-Rotors*; Wiley: New York, 1963.

(36) Wu, Y. R.; Levy, D. H. Determination of the geometry of deuterated tryptamine by rotationally resolved electronic spectroscopy. *J. Chem. Phys.* **1989**, *91*, 5278.

(37) Holland, J. H. *Adaption in Natural and Artificial Systems*; The University of Michigan Press: Ann-Arbor, 1975.

(38) Goldberg, D. E. *Genetic Algorithms in search, optimisation and machine learning;* Addison-Wesley: Reading, MA, 1989.

(39) Rechenberg, I. *Evolutionsstrategie-Optimierung technischer Systeme nach Prinzipien der biologischen Evolution*; Frommann-Holzboog: Stuttgart, 1973.

(40) Stein, S. E.; Rabinovitch, B. S. Accurate evaluation of internal energy level sums and densities including anharmonic oscillators and hindered rotors. *J. Chem. Phys.* **1973**, *58*, 2438.

(41) Spangenberg, D. Strukturelle und kinetische Untersuchungen an H-brückengebundenen ionischen Clustern des Phenols, Dissertation, Heinrich-Heine-Universität, Math. Nat. Fakultät, Düsseldorf, 2000.

(42) Scoles, G., Ed. *Atomic and Molecular Beam Methods*; Oxford University Press: New York, Oxford, 1988; Vol. 1.

(43) McWhorter, D. A.; Hudspeth, E.; Pate, B. H. J. The rotational spectra of single molecular eigenstates of 2-fluoroethanol: Measurement of the conformational isomerization rate at 2980 cm^{-1}. *J. Chem. Phys.* **1999**, *110*, 2000.

JP8087989